

## Vortex Tracking Algorithm for Hypersonic Flow in Scramjets

J. R. Llobet, J. E. Barth and I. H. Jahn

Center for Hypersonics  
 University of Queensland, Queensland 4072, Australia

### Abstract

Hypersonic airbreathing propulsion for access to space has several advantages over conventional rockets. However, to achieve the theoretical propulsion efficiencies, many technological challenges, such as fast and efficient mixing of the fuel with air, still need to be resolved. Several scramjet inlet geometries naturally generate vortices that could be used for mixing enhancement. Thorough characterization of these vortices is required for studying their effect on mixing and to determine the optimum way to utilize these naturally occurring vortical flow structures. For this purpose, an algorithm that tracks and extracts data along a vortex from a computational fluid dynamics (CFD) flow field solution was implemented. It performs a search in slices of the computational solution, based on Galilean-invariant criteria for vortices. The algorithm has been used to analyse the vortices generated by compression corner and within a real scramjet inlet. Results are presented showing the insight in vortex formation and evolution provided by the algorithm.

### Introduction

By using the oxygen in the atmosphere, hypersonic airbreathing engines such as scramjets are not required to carry both fuel and oxidizer. This presents an increase in specific impulse and payload mass fraction compared to rocket based launchers [1] [2]. However, the high supersonic flow velocities inside the engine and thus low residence times ( $< 1$  ms) pose several challenges. One of them is fast and efficient fuel mixing, a pre-requisite to fast and efficient combustion. In order to have short combustors, required to keep skin friction losses and heat transfer at a minimum, fast mixing and burning is essential [3]. Therefore, mixing enhancements for hypersonic engines are an active topic of research. Currently, different injection strategies such as hypermixers or utilisation of inlet generated vortices are studied for this purpose.

In the later case, the interaction between the vortices generated by scramjet inlet and the porthole fuel jets, situated towards the end of the scramjet inlet, are expected to significantly improve mixing efficiency. Currently, investigation on this process is ongoing at University of Queensland (UQ). One or more of the following mechanisms of mixing enhancement as a result of the vortex-fueljet interaction are expected by the authors:

- Convection of the fuel away from the injector location by the rotating flow of the stream-wise vortex.
- Increased penetration of the fuel due to the reduced pressure in the vortex core.
- Bursting of the vortex, provoked by the interaction between stream-wise vortex fuel plume bow-shock. Such bursting is documented to produce a high turbulence region [10] and this increases turbulent mixing.

To study the mixing enhancement, the characterisation of the stream-wise vortical structure that interacts with the fuel jet is essential. Specifically the size and intensity of the vortex, and the pressure and velocity fields at its core are of interest.

	Mach	$P_0$	$T_0$	Enthalpy
Simple	10	89.5 MPa	5140.5 K	$5.33 \text{ MJ kg}^{-1}$
REST	12	75.0 MPa	6487.5 K	$6.5 \text{ MJ kg}^{-1}$

Table 1: Flow boundary conditions

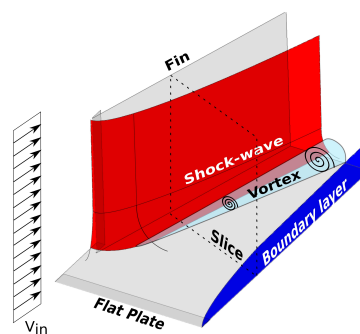


Figure 1: Flat plate and fin vortex generation.

This paper reports the development of an algorithm developed to analyse stream-wise vortex structures. In addition the results obtained from vortex analysis performed for a simplified geometry which generates an inlet-like vortex, and for the Rectangular-to-Elliptical Shape Transition (REST) inlet developed by Smart [8] are presented.

### Test geometries

The development of the vortex characterisation algorithm is explained based on two test geometries which are presented next. First, a simple geometry for testing the algorithm in a relatively simple flow-field. Second, the REST inlet geometry to show the potential of the code to track and extract valuable information from realistic complex flow-fields. Flow boundary conditions used for the two geometries are given in table 1.

#### Simplified test geometry

The simplified geometry is a flat plate with a sharp fin at a  $15^\circ$  compression angle. The viscous-shock interaction between the flat plate boundary layer and the fin shock-wave generates a corner vortex (Figure 1). The flow-field present a conical flow-field a certain distance downstream of the fin leading edge, named "inception zone" in [11]. This simple geometry generates a vortex in a similar fashion and with a similar velocity field in the vortex core as those generated by real scramjet inlets.

#### REST inlet

The REST inlet, developed by Smart [8] is currently under development at UQ. Here the rectangular capture area, that transitions to an elliptical cross-section (Figure 2), allows efficient airframe integration of the engine while maintaining an efficient elliptical combustor cross-section. For the current investigation, RANS CFD results generated by Barth et al. [9] are used.

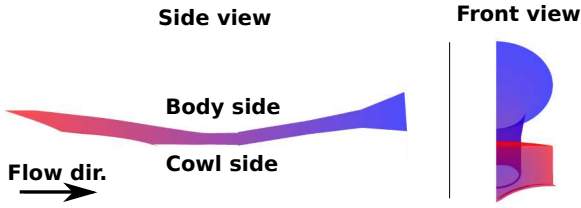


Figure 2: REST engine geometry, from [9].

### Vortex tracking algorithm

The tracking algorithm extracts data along individual macroscopic vortices. To achieve this in the first step the algorithm searches a user supplied slice extracted from the flow-field, detecting the vortex core and vortex edge using one of several vortex detection criteria. Once the vortex has been identified, the code automatically tracks the vortex to its inception/end by iteratively generating slices upstream/downstream based on local flow and vortex properties.

### Vortex criteria

To detect vortices three Galilean invariant methods are implemented. These generate a scalar field based on calculations performed on the velocity gradient tensor ( $J$ ), and indicate the presence and strength of vortices. Being Galilean invariant they are not affected by coordinate system orientation. The different criteria use the velocity tensor,  $J$ , or its symmetric part, obtained by braking it down into its symmetric,  $S^2$ , and anti-symmetric,  $\Omega^2$ , components:

$$\left(S^2 + \Omega^2\right) = J, \quad (1)$$

From this the three criteria are defined as:

**Q factor** Vortex is as a region with a positive second invariant of  $J$  [4].

$\lambda^2$  Vortex is defined as a region where the eigenvalues of  $S$  are negative [5]

**Critical point** Vortex is as a region with two complex eigenvalues in  $J$  [6]. Moreover, the direction of the rotation axis is given by the eigenvector associated with the real eigenvalue [6].

Results from the three criteria applied to a slice taken from the simple geometry, 45.0mm downstream of the fin leading edge are shown in figures 4a to 4d. The bottom side corresponds to the flat plate wall, the left hand side correspond to the fin wall.

### Detection

Vortex detection is performed on a slice-by-slice basis. For the first step the slice is user defined using a point and plane normal. In subsequent steps these values are determined automatically as defined in the Stepping section. Within any slice the algorithm then calculates the selected criterion ( $\lambda^2$ , Q factor, or Critical Point) for the whole slice (see Fig. 4a to Fig. 4d). Here regions of high scalar criterion values present vortex regions. On the first slice the user can manually select the desired vortex to be tracked if there are more than one vortex present in the flow-field.

Once the vortex region to be tracked is selected, the algorithm starts searching around the desired location to identify the vortex core center and the vortex core edge. The core center is defined as the maxima of the criterion value within the selected region, resulting in  $C_{core}$ . The core edge is either defined using the criterion definition or as a fraction of the core centre

value. In the later case, only points exceeding a threshold fraction,  $R_{e/c}$  defined as

$$R_{e/c} = \frac{C_{edge}}{C_{core}}, \quad (2)$$

where  $C_{edge}$  is the criterion value at the core edge, are selected to fall within the vortex core. To track a single vortex, the maxima (core center) is only searched for within the vortex region defined by the core edge. Therefore, as  $R_{e/c}$  is fixed and as the the edge threshold value,  $C_{edge}$ , and center value,  $C_{core}$ , are linked by equation 2, and the center is only searched within the region closed by the vortex, both the center and edge have to be evaluated simultaneously. For this, the algorithm starts by evaluating a small area around the prospective vortex center (indicated by the user or estimated from the data in a previously evaluated slice). If the new evaluated area contains a discrete point with a higher maxima for the criteria value, the prospective vortex center location is updated. Hence, the threshold value for the edge detection is also updated. Next a new edge location is obtained by searching for the limit of the area satisfying the threshold value. Here if the evaluated area is increased until closed edge is identified. This process is exemplified in Fig. 3, where the searched area increases until the vortex edge is fully contained. In this simple case, the vortex center is kept constant. However, if the new area contained a higher maxima, the core center (Prospective point in Fig. 3) would be updated.

### Stepping

Once the core centre and core edge are obtained, the algorithm advances to the next slice. The stepping direction to advance to the new plane and its orientation are selected based on the flow values of the vortex core center in the current slice. Three stepping criteria are implemented: vorticity vector, velocity vector, and eigenvector. The velocity vector is more suitable than the vorticity for the investigated vortices, as they are primarily convected by the core flow. Therefore the velocity vector is a good predictor for the convected new location of the core center upstream or downstream. Moreover, the proximity to the boundary layer can distort the vorticity vector. Alternatively, in the case of the Critical Point criterion, the eigenvector corresponding to the real eigenvalue of the tensor  $J$  can be used as the stepping direction.

The next slice point is obtained stepping in the selected vector direction from the current vortex core center. The plane normal is parallel to this vector. This allows for visualization of the rotating vortex core flow pattern, as the tangential and radial components of the velocity about the vortex center are captured by the plane.

### Data extraction

In addition to tracking the vortex core and core edge location, in each slice, the fields of velocity, pressure, temperature and Mach number are also extracted. Post-processing of this data allows the path of the vortex core to be reconstructed by joining the vortex core center locations between slices. The vortex core area can be visualized by plotting the edge extracted from the slices. The tangential, radial and axial velocities about the vortex core center are also calculated. Moreover, the streamwise evolution of the mean radius ( $R_{mean}$ ) and area ( $A$ ), criterion value at the core center, streamwise velocity at the vortex core center ( $U_{core}$ ), circulation ( $\Gamma$ ), vortex intensity parameter ( $V.I. = \Gamma / (U_{core} \cdot R_{mean})$ ) [7], and angular momentum ( $L$ ) of the flow within the vortex core are calculated for each streamwise location.

Performing this analysis provides a clear picture of how the vortex properties evolve, starting from the vortex inception.

## Results

### Simple test case

The vortex tracking algorithm has been tested in the simple geometry described above. Results for vortex intensity (Fig. 5a), vortex area (Fig. 5c), stream-wise velocity in the vortex core (Fig. 5e), and angular momentum (Fig. 5g) are presented.

The three different criteria are compared in the plots. The threshold for the edge detection for the Q factor and Critical Point criteria was set to  $R_{e/c} = 0.2$ . Values lower than  $R_{e/c} = 0.2$  generate excessive vortex areas, cause adjacent but independent vortices to be included. For the  $\lambda_2$  criterion  $R_{e/c} = 0.5$ . This value avoids the vortex area extending to the flat plate wall, where a high  $\lambda_2$  value region is present (Fig. 4c), which distorts the tracking.

The different criteria and different threshold values provide different vortex areas. Therefore, comparison amongst different criteria can only be qualitative. The evolution of vortex intensity, vortex area and angular momentum shows three distinct vortex regions. The first is the vortex initiation zone (*I*), extending from the vortex inception to about 0.02 m downstream of the fin leading edge. In this region the vortex intensity, vortex area and angular momentum evolve following a polynomial curve of order 3, 1 and 2 respectively. A transition zone (*II*), where the vortex area remains relatively unchanged, extends approximately from 0.02 m to 0.045 m. The developed vortex area (*III*) shows a fully formed vortex growing conically, where the vortex intensity, vortex area and angular momentum evolve following a polynomial curve of order 1, 2 and 3 respectively. It extends from about 0.045 m downstream of the fin leading edge to the end of the computational domain.

The quadratic growth of the vortex in the developed zone agrees with the conical evolution of the flow-field, as the radius of the vortex increases linearly. Equation 3 shows that for small variation of density ( $\rho$ ) and tangential velocity ( $v_t$ ), angular momentum is expected to grow cubically with the vortex radius. The vortex intensity is constant in the developed region as the increase in circulation is balanced by the increase in vortex radius. The evolution of the vortex core center velocity shows how the core of the vortex moves from the low region of the boundary layer, where the stream-wise velocity is almost zero, to the outer part, where the stream-wise velocity is close to the free-stream.

$$L = \int^S r \cdot v_t \cdot \rho \cdot ds \quad (3)$$

### REST inlet

After obtaining satisfactory results in the simple flow-field generated by the simple geometry, the algorithm was tested on a real scramjet flow-field. For this purpose the RANS CFD solution obtained by Barth et al. [9] is used. The results shown in Fig. 5b, 5d, 5f, and 5h are obtained for the most upstream vortex generated by the inlet.

The REST inlet vortex shows a significant similarity in its evolution to the vortex in the simple geometry between its inception in  $X = 0.05$  m to approximately  $X = 0.125$  m. Downstream of this axial location the complex flow-field distorts the evolution of the vortex. Despite the spikes that arise due to secondary shock-waves traversing the flow-field, the initial zone of the REST vortex shows a quasi linear growth of the vortex area. The angular momentum grows in a quadratic fashion. Moreover, the evolution of ( $U_{core}$ ) (Fig. 5f) also shows the migration of the vortex core from the lower part of the boundary layer to the outer part. This migration distance seems to drive the length of the initiation zone (*I*). Even though  $U_{core}$ , *V.I.* and *A* show the

same trends in both cases, the vortex intensity (Fig. 5b) shows a different trend. The three terms on which *V.I.* depends ( $\Gamma$ ,  $U_{core}$ , and  $R_{mean}$ ) show similar evolution in both cases. Therefore, this difference is explained by a higher increase rate in  $U_{core}$ , and  $R_{mean}$  in relation with the  $\Gamma$  than for the simple case.

## Conclusions

A vortex tracking algorithm has been presented. Results on a simplified scramjet inlet geometry showed the capability of the algorithm to provide deep insight in the vortex formation and evolution. Testing the code on a real scramjet flow solution (RANS CFD) showed the ability of the code to track vortices in a highly complex flow-field. This capabilities will be used in the characterization of vortex-injection interactions which are expected to allow gains in mixing efficiency for hypersonic air-breathing engines, specifically scramjets.

## Acknowledgements

This research was supported under Australian Research Council's Discovery Projects funding scheme (Project DP130102617 - The science of scramjet propulsion). The author would also like to thank the School of Mechanical and Mining Engineering at UQ, for the financial support.

## References

- [1] Smart, M. K. & Tetlow, M. R., Orbital delivery of small payloads using hypersonic airbreathing propulsion, *J. Spacecraft Rockets*, **46**, No.1, 2009, 117-125.
- [2] Cook, S. & Hueter, U., NASA's integrated space transportation plan 3rd generation reusable launch vehicle technology update, *Acta Astronautica*, **53**, 2003, 719-728.
- [3] Fuller, R. P., Wu, P. K., Nejad, A. S. & Schetz, J. A., Comparison of physical and aerodynamic ramps as fuel injectors in supersonic flow, *J. Propul. Power*, **14**, No.2, 1998, 135-145.
- [4] Hunt, J. R. C., Wray A. A. & Moin, P., Eddies, streams, and convergence zones in turbulent flows, *CTR, Proceedings of the Summer Program*, 1988, 193-208.
- [5] Jeong, J. & Hussain, F., On the identification of a vortex, *J. Fluid Mech.*, **258**, 1995, 69-94.
- [6] Chong, A. E., Perry, A. E. & Cantwell, B. J., A general classification of three-dimensional flow fields, *Phys. Fluids*, **2**, 1990, 765-777.
- [7] Kalkhoran, I. M., Vortex distortion during vortex-surface interaction in a Mach 3 stream, *AIAA Journal*, **32**, No.1, 1994, 123-129.
- [8] Smart, M. K., Design of three-dimensional hypersonic inlets with rectangular-to-elliptical shape transition, *J. Propul. Power*, **15**, No.3, 1999, 288-293.
- [9] Barth, J. E., Wheatley, V., Smart, M. K., Petty, D. J., & Basore, K. D., Flow physics inside a shape-transitioning scramjet engine, *18th AIAA/3AF ISPHSTC*, 24-28 September, Tours, France 2012.
- [10] Smart, M. K., Kalkhoran, I. M. & Betti, A., Interaction of supersonic wing-tip vortices with a normal shock, *AIAA Journal*, **34**, No.9, 1996, 1855-1861.
- [11] Settles, G. S. & Lu, F. K., Conical, Conical similarity of shock/boundary-layer interactions generated by swept and unswept fins *AIAA Journal*, **23**, No.7, 1985, 1021-1026.

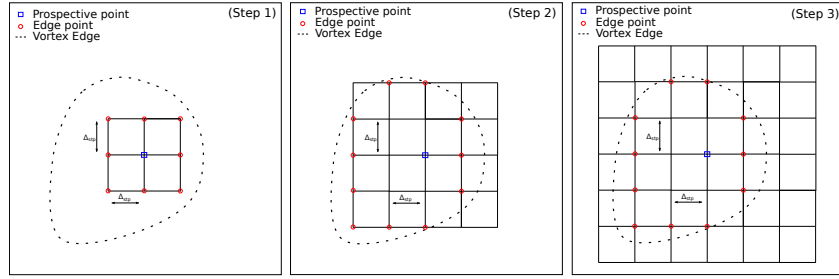


Figure 3: Vortex edge and center detection example.

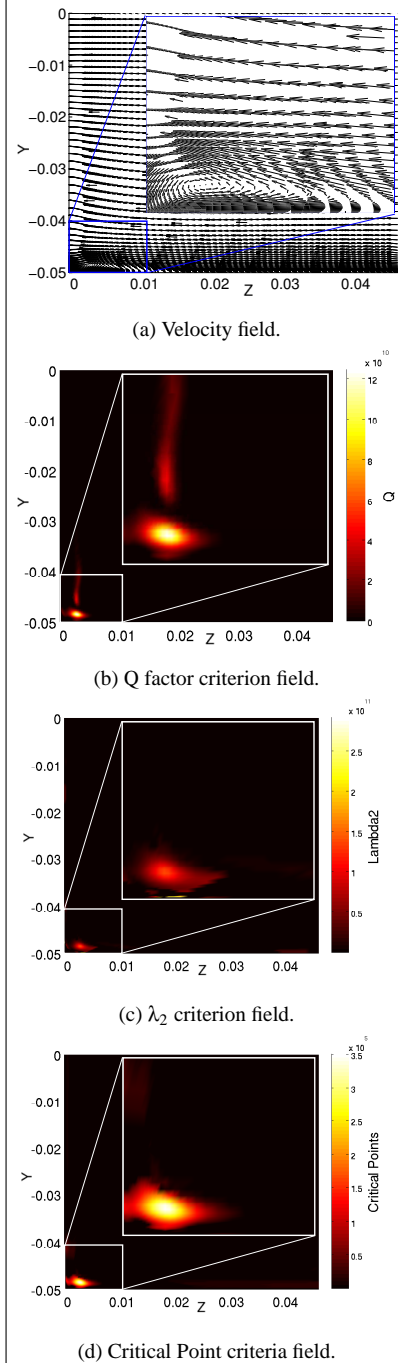


Figure 4: Velocity and criteria fields on a single slice from the simple geometry 45.0mm downstream of the fin leading edge and with its normal forming a  $20^\circ$  angle with the axial direction.

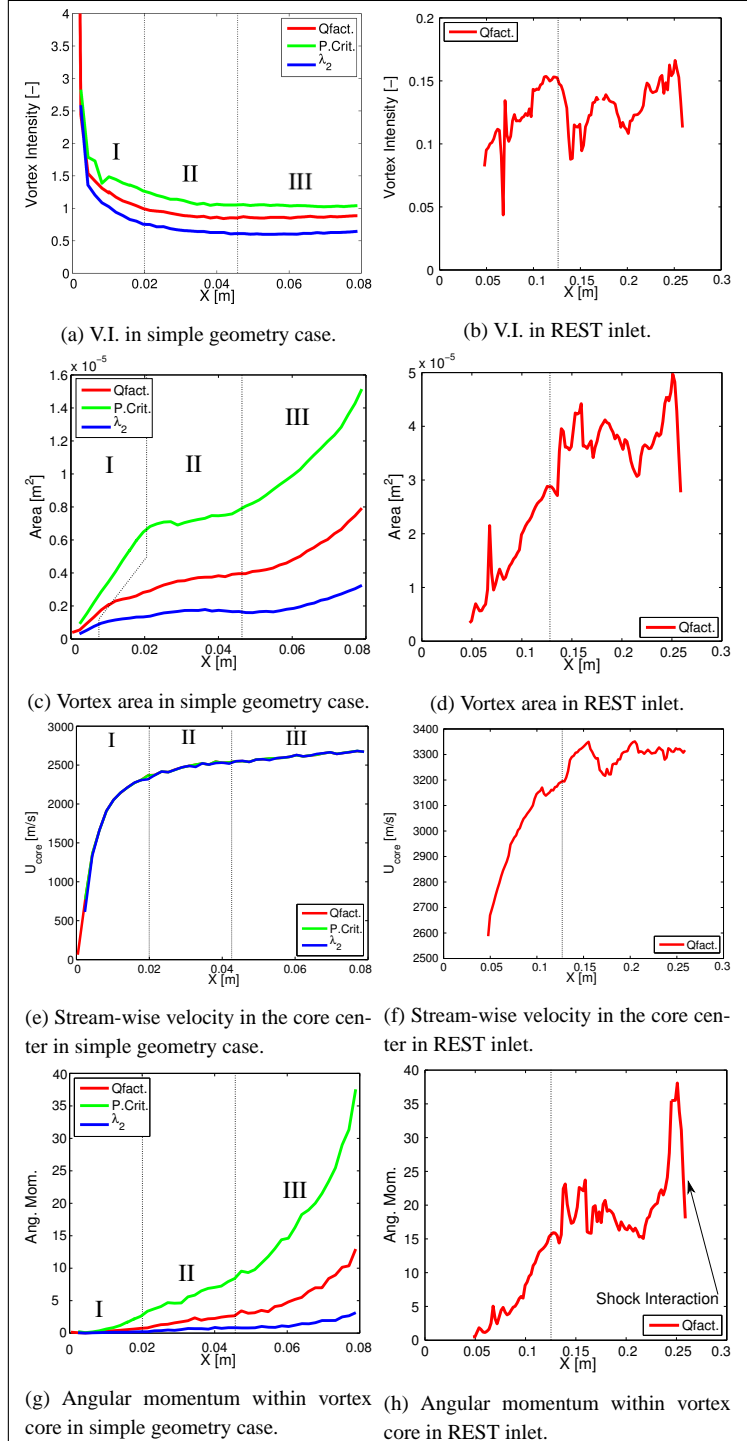


Figure 5: Vortex development plots for the simple and REST inlet geometries.